

Short Communication

Electrochemical Corrosion Behavior of TiN-coated 310S Stainless Steel in an Electric Water Heater in a Simulated Environment

Zhong Yin

Guangdong Midea Group Co., Ltd., Foshan 528311, Guangdong Province, China

E-mail: ZYin_Midea@163.com

Received: 5 November 2021 / *Accepted:* 16 December 2021 / *Published:* 5 January 2022

A uniform and dense TiN coating was successfully prepared on the 310S stainless steel by magnetron sputtering. The morphologies and chemical composition of the TiN coating were analyzed by using scanning electron microscopy (SEM) and X-ray diffraction (XRD). The electrochemical corrosion behavior was investigated in a simulated electric water heater environment. The results reveal that the TiN coating exhibits good stability in synthetic tap water and 3.5% NaCl solution at 80 °C. The values of polarization resistance, corrosion potential and pitting potential of TiN-coated 310S stainless steel are much higher than those of the 310S substrate. It is suggested that TiN coatings can provide excellent corrosion resistance for 310S stainless steel in an aggressive environment containing chloride ions.

Keywords: 310S stainless steel; TiN coating; Electrochemical corrosion; Tap water

1. INTRODUCTION

Electric storage water heaters are widely used in daily life and are mainly composed of inner tanks and heating tubes. As a major component of electric storage water heaters, heating tubes operate in a complex variable temperature environment for long periods. In general, the internal temperature of the heating tube is approximately 200~300 °C, the temperature in the tube near the water is approximately 100 °C, and the water temperature is in the range of 25~80 °C. In addition, the water quality varies significantly in different regions, and the water generally contains chloride ions. However, the actual working status of the heating tubes is difficult to monitor, so corrosion failure events occur frequently. Corrosion of the heating tubes often shortens the service life of the electric water heater. Additionally, once the heating tubes burst and leak, there is a risk of electric shock to the human body. Therefore, reducing the corrosion risk of heating tubes is a critical problem for the safe use of electric water heaters, and this topic has attracted increasing attention from the electric water heater industry.

At present, 300 series stainless steels (e.g., 316L and 310S) are widely used in heating tubes for electric water heaters because of their excellent mechanical properties and corrosion resistance. However, the design life of an electric water heater is usually as long as 8 to 10 years, so corrosion of the stainless steel heating tubes is still inevitable. Fabricating various protective coatings on stainless steel surfaces to reduce the corrosion rate is a widely used method in the industry [1-10].

Titanium nitride (TiN) coatings have been widely applied in several fields due to their high hardness, wear resistance and low friction coefficient [11-14]. In addition, TiN coatings are also corrosion resistant and have metal-like thermal conductivity characteristics [15]. The corrosion behavior of TiN coated metallic materials has also been widely investigated in some application environments [16-20]. Liu et al. showed that TiN-coated 316L stainless steel showed a lower corrosion tendency and higher corrosion resistance than the bare substrate in simulated bodily fluid [21]. Chu et al. prepared multilayered Ti/TiN and single TiN coatings on NiTi alloys by pulse-biased arc ion plating and found that the coatings displayed much higher corrosion potential and impedance and lower passive current density in artificial saliva [22]. In the past decade, most of the research on the corrosion behavior of TiN coatings has focused on the fuel cell environment of the proton exchange membrane [17, 22-26]. To date, there is still little information on the corrosion properties of TiN coated stainless steel in hot tap water environments that appear in electric water heaters.

In this paper, a TiN film was coated on 310S stainless steel using magnetron sputtering technology and the electrochemical corrosion behavior of the coated material was investigated in synthetic tap water. The results will provide fundamental information on the corrosion performance and the application of TiN film in heating tubes.

2. EXPERIMENTAL

2.1 Materials and solution

A commercial 310S stainless steel plate (0.5 mm in thickness) with a chemical composition (wt.%) of C 0.045, Si 0.74, Mn 1.21, S 0.003, P 0.023, Cr 23.91, Ni 19.02, N 0.17 and Fe balance was used. The specimens were fabricated into 11×11 mm pieces by electric discharge machining and then cleaned with acetone to remove contaminants. Prior to the deposition process, the substrates were polished with 400 to 1000 grit SiC waterproof abrasive papers and then ultrasonically cleaned in anhydrous ethanol and distilled water. After that, the specimens were dried in cold air for later use.

The TiN coatings were deposited by utilizing a high vacuum magnetron sputtering system (JGP 280). In the electrochemical corrosion tests, the TiN coating and uncoated specimens were embedded in epoxy resin with an exposed area of approximately 1 cm². Before the electrochemical experiments, the TiN-coated specimen was rinsed with ethanol and distilled water, and the uncoated specimen was ground slightly with 1000 grit SiC paper and then cleaned in the same way.

To obtain more information about the electrochemical corrosion behavior of the TiN coating, synthetic tap water and 3.5% NaCl solution were used for the electrochemical tests. Synthetic tap water was prepared according to the results of a literature study [27] that involved the analysis of 75 samples

of tap water collected from 25 typical urban regions in China. The chemical composition of synthetic tap water is listed in Table 1. The pH was adjusted to approximately 7.6 by using 0.5 M H₂SO₄ solution. All the tests were conducted at 80 ± 1 °C (i.e., the maximum water temperature inside the electric water heater).

Table 1 The chemical composition of the test solution (mg L⁻¹)

Cl ⁻	SO ₄ ²⁻	HCO ₃ ⁻	Ca ²⁺	Mg ²⁺
0.045	0.74	1.21	0.003	0.023

2.2 Electrochemical experiments

All electrochemical tests were conducted in a three-electrode cell through a Princeton electrochemical workstation (Versa STAT 3F). The specimen was used as the working electrode, and a saturated calomel electrode (SCE) with a salt bridge and a platinum plate (20 × 20 mm) were used as the reference electrode and the auxiliary electrode, respectively. The corrosion potential was first recorded for 60 min to attain a relatively stable surface state after the specimen was immersed in the test solution. After that, electrochemical impedance spectroscopy (EIS) was conducted at the corrosion potential with an AC disturbance signal of 10 mV (rms) in the frequency region of 99 kHz-10 mHz. All impedance data were analyzed using ZsimpWin software. Finally, the potentiodynamic polarization curves were recorded from the corrosion potential at a scan rate of 20 mV min⁻¹ until the current density reached 100 μA cm⁻². The electrochemical tests were repeated at least three times with different specimens.

2.3 Surface analysis

The coated specimen was examined by X-ray diffraction (XRD) using a Rigaku diffractometer (D/MAX 2550 V) with Cu Ka radiation. The scanning rate was 4° min⁻¹ for 2θ in the range of 10° to 90°. The surface and cross-sectional microstructures of the TiN coating were characterized by electron microscopy (SEM, HITACHI S3400).

3. RESULTS AND DISCUSSION

3.1 Microstructure characteristics of TiN coating

Fig. 1 presents the XRD patterns of the uncoated and TiN-coated 310S stainless steel. Both the 310S substrate and TiN coating had an FCC structure. The diffraction peak intensity of the austenite substrate in the TiN-coated specimen noticeably weakened. The main diffraction peaks of the TiN coating are (1 1 1), (2 0 0), (2 2 0) and (3 1 1). In addition, the (1 1 1) diffraction peak is stronger than that of (2 0 0), which can be attributed to the fact that the TiN coating mainly grows along the <1 1 1>

direction with a columnar structure [16, 28, 29]. These results are in accordance with reports in the literature [16, 17, 30, 31].

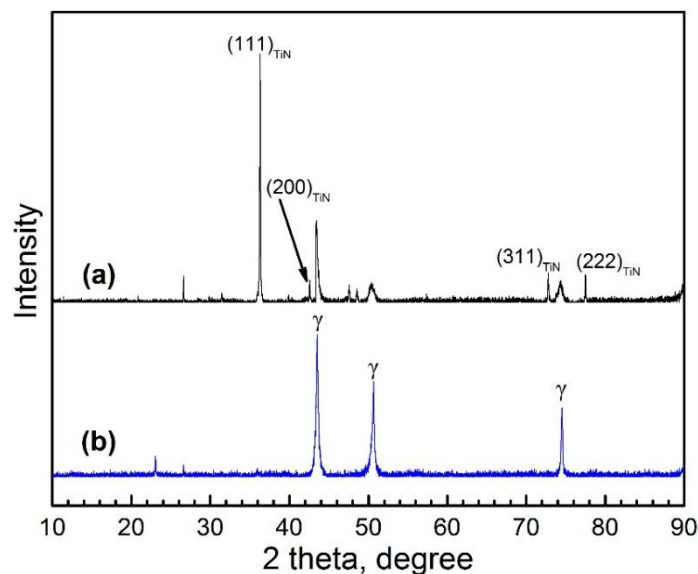


Figure 1. XRD patterns of (a) TiN coated and (b) uncoated 310S stainless steel

Fig. 2 shows the planar and cross-sectional SEM micrographs of the TiN coating prepared on the 310S stainless steel surface. The TiN coating presents a uniform and dense microstructure. There are some spindle- or round-shaped microparticles on the TiN surface, which is similar to the result in the literature [30]. The cross-sectional morphologies in Fig. 2b show that the coating/substrate interface is well defined and that the thickness of the TiN coating is approximately 7 μm .

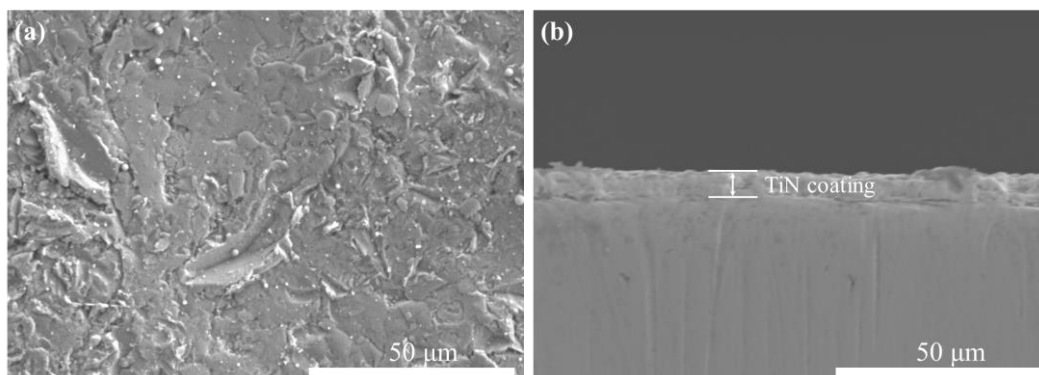


Figure 2. The planar (a) and cross-sectional (b) SEM micrographs of the TiN coating

3.2 Electrochemical corrosion characteristics

Fig.3 shows the typical EIS curves of the TiN coating and 310S stainless steel substrate after 1 h of immersion in synthetic tap water and 3.5% NaCl solution at 80 $^{\circ}\text{C}$. The Nyquist plots present a similar

impedance characteristic with an incomplete capacitive semicircle. It is apparent that the semicircle sizes of the TiN coating in both test solutions are much larger than those of the 310S stainless substrate. In synthetic tap water, the time constants from the charge transfer process in the low-frequency region and passive film in the high-middle-frequency part overlap together and show one θ peak in the Bode curves. This result is similar to the results for 444 stainless steel in hot tap water [27]. Moreover, the θ value of the coated specimen is slighter than that of the uncoated specimen. For the 3.5% NaCl solution, the two time constants overlapped as a horizontal platform. This result is in accordance with the results reported in the literature [32-34]. In addition, both the θ value and frequency range of the horizontal platform for the TiN coating are larger than those of the 310S substrate.

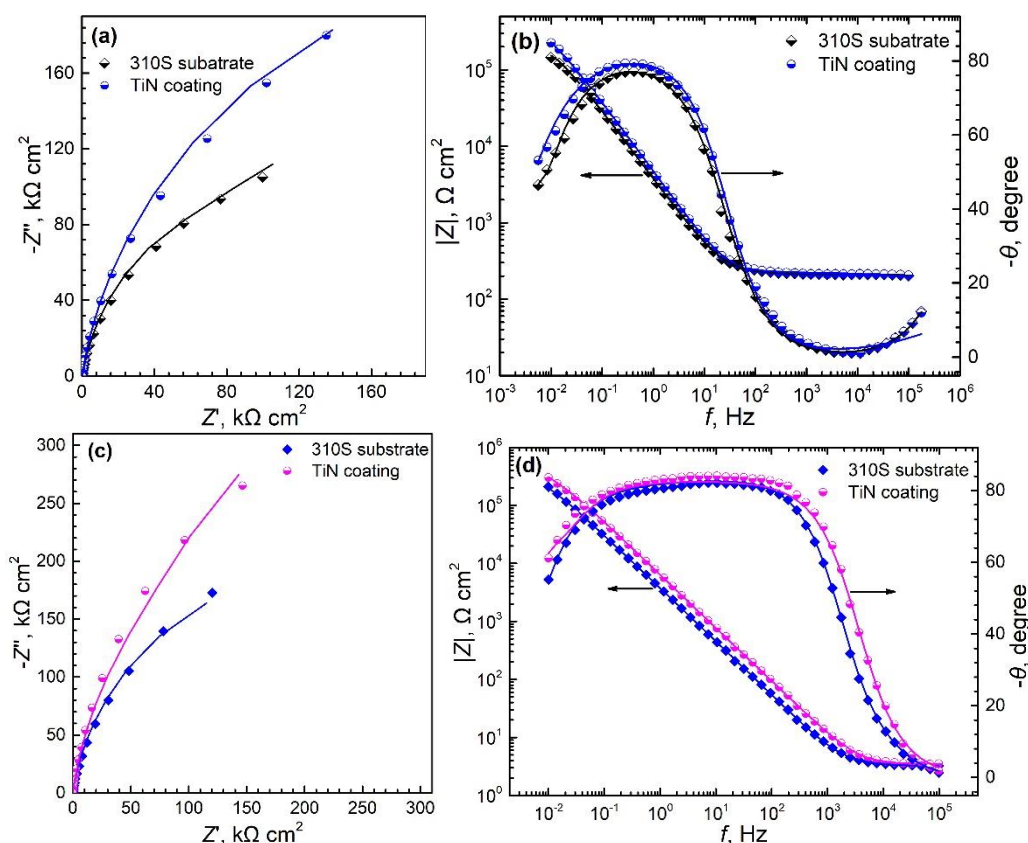


Figure 3. Typical EIS plots (a, c) Nyquist and (b, d) Bode for the specimens in (a, b) synthetic tap water and (c, d) 3.5% NaCl solution at 80 °C

Based on these characteristics, the equivalent circuit displayed in Fig. 4 was adopted to fit the EIS spectra in Fig. 3, where R_s represents the solution resistance, R_f and C_f represent the resistance and capacitance of the passive film, and R_t and C_{dl} represent the charge transfer resistance and double layer capacitance, respectively [34]. Due to the nonideal capacitive response of the stainless steel/solution interface, all the capacitance elements were replaced by the constant phase element (CPE) in the fitting process [8, 34, 35]. The impedance of CPE can be expressed as follow:

$$Z_{CPE} = \frac{1}{Y_0(j\omega)^n}$$

where Y_0 is the admittance magnitude of CPE and n is the exponential term [34, 35].

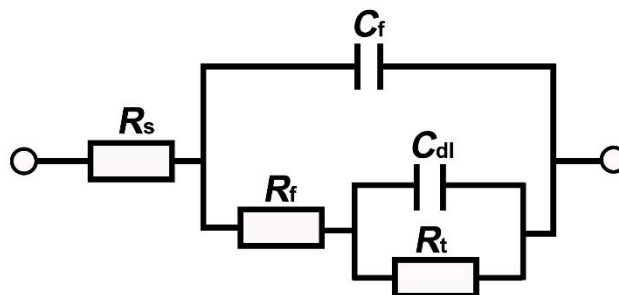
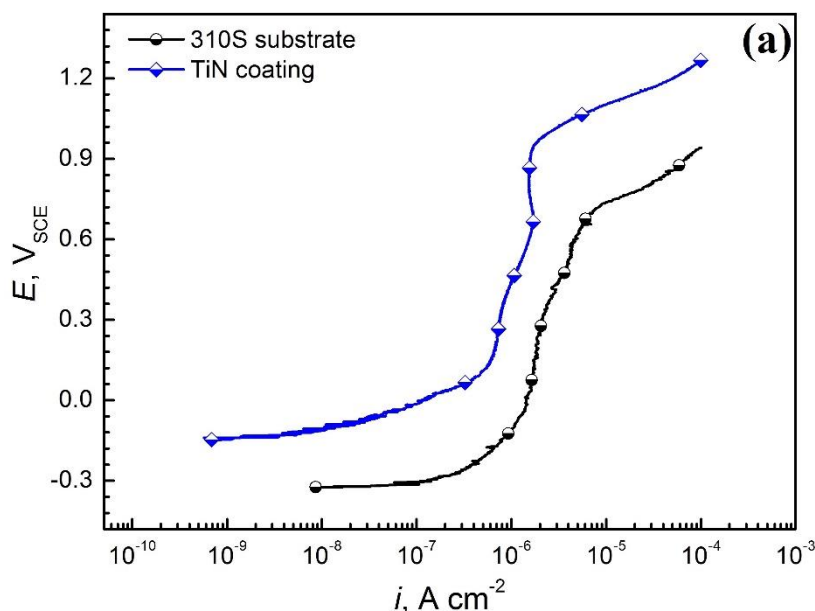


Figure 4. Equivalent circuit for the electrode system stainless steel/NaCl solution

Table 2. The fitted results of EIS spectra in synthetic tap water and 3.5% NaCl solution.

Specimen	R_s (Ωcm^2)	Y_{0-f} ($10^{-5}S^\alpha \Omega \text{cm}^{-2}$)	n_f	Y_{0-dl} ($10^{-5}S^\alpha \Omega \text{cm}^{-2}$)	n_{dl}	R_p ($k\Omega\text{cm}^2$)
<i>Synthetic tap water</i>						
310S	198.2	9.69	0.87	9.85	0.87	333.4
TiN coating	201.1	5.18	0.89	4.06	0.91	629.5
<i>3.5% NaCl solution</i>						
310S	3.2	6.34	0.91	5.33	0.86	453.2
TiN coating	3.5	2.81	0.93	3.31	0.91	824.2

Table 2 presents the fitted results of the parameters. According to the literature, the polarization resistance R_p , which represents the corrosion resistance, can be theoretically calculated by taking the sum of R_f and R_t [8, 34, 35].



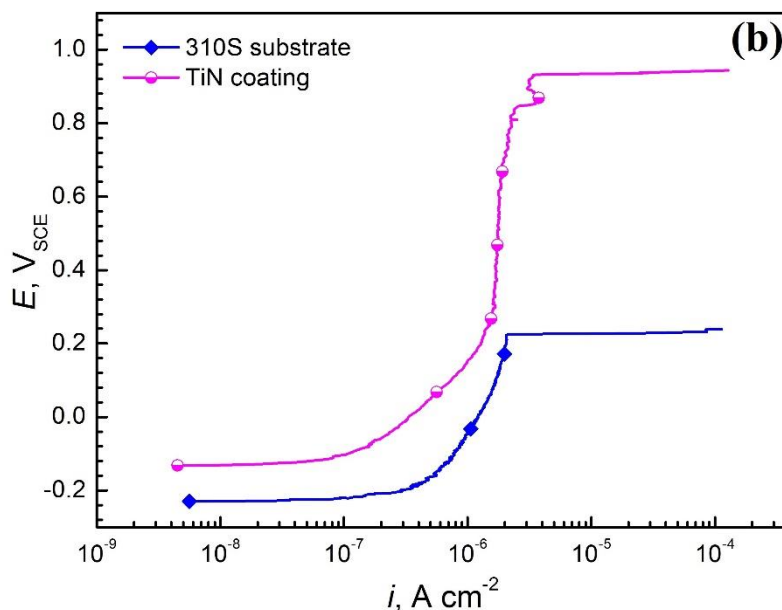


Figure 5. Anodic polarization curves for the specimens in (a) synthetic tap water and (b) 3.5% NaCl solution at 80 °C

In comparison with 3.5% the NaCl solution, the R_s value (approximately $200 \Omega \text{ cm}^2$) is apparently higher due to the low conductivity of the synthetic tap water. Both the TiN coated and uncoated 310S stainless steel specimens have large R_p values on the order of $10^5 \sim 10^6 \Omega \text{ cm}^2$ in the test solutions at 80 °C. Moreover, compared to those of the 310S substrate, the R_p values of the TiN-coated specimen are much larger, whereas the Y_{0-f} and Y_{0-dl} values are clearly lower. Fig. 5 gives the potentiodynamic polarization curves for the specimens in synthetic tap water and 3.5% NaCl solution at 80 °C, and the corresponding electrochemical parameters are listed in Table 3. Both the coated and uncoated 310S stainless steel specimens can passively spontaneously in the test solutions. In comparison with those of the uncoated specimens, the passive current density of TiN-coated specimens was obviously lower and the corrosion potential (E_{corr}) was higher in both test solutions. In synthetic tap water, the current density of the 310S substrate increased noticeably when the applied potential reached approximately 700 mV_{SCE}, which corresponds to the oxygen evolution in the reaction: $2\text{H}_2\text{O} + 4\text{e}^- \rightarrow \text{O}_2 + 4\text{H}^+$ [36, 37]. For the TiN-coated specimen, the oxygen evolution potential (E_{evo}) increased to approximately 950 mV_{SCE}. It is believed that the oxygen evolution on the specimen surface could reduce the pitting sensitivity of stainless steel [38].

However, the anodic polarization curves measured in 3.5% NaCl solution displayed some different characteristics, as shown in Fig. 5 (b). The current density enlarged suddenly when the applied potential was increased to a critical value, indicating the occurrence of stable pitting corrosion on the electrode surface and the corresponding potential was defined as the pitting potential (E_p). The E_{corr} and E_p values of the TiN-coated specimen were clearly higher than those of the 310S substrate specimen, which agrees with the EIS results. The E_p value of the 310S substrate shifts positively from 231 ± 26 to 951 ± 15 mV_{SCE}, whereas the ΔE ($\Delta E = E_p - E_{\text{corr}}$) value enlarges from 474 ± 18 to 1089 ± 23 mV. The

obviously higher E_{corr} and E_p values and much larger passive region indicate a tremendous improvement in the pitting resistance of 310S stainless steel by the TiN coating.

Table 3. The corrosion parameters extracted from Fig. 5.

Sample solution	Coated		Uncoated	
	Synthetic tap water	3.5% NaCl	Synthetic tap water	3.5% NaCl
E_{corr} (mV _{SCE})	-142 ± 10	-143 ± 6	-353 ± 16	-237 ± 5
E_{evo} or E_{pit} (mV _{SCE})	942 ± 8	951 ± 15	704 ± 15	231 ± 26
ΔE (mV)	1084 ± 14	1089 ± 23	1039 ± 27	474 ± 18

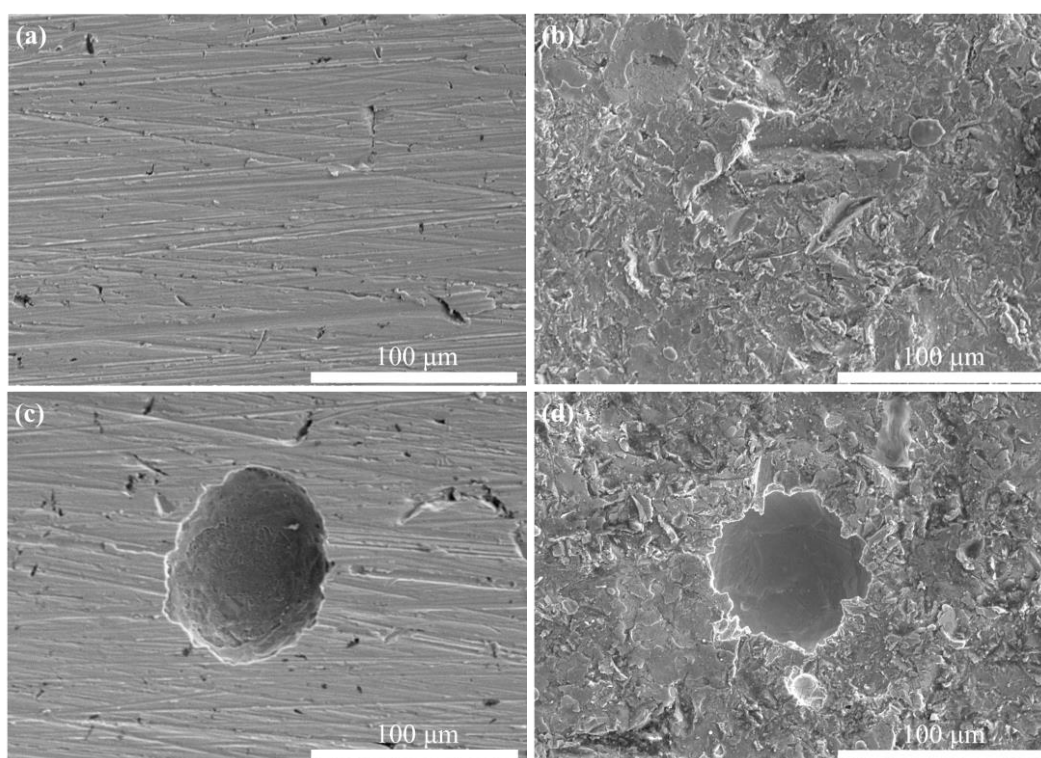


Figure 6. SEM morphologies of the specimen surfaces after the polarization measurement: (a, b) in the synthetic tap water, (c, d) in 3.5% NaCl solution; (a, c) for uncoated specimens, (b, d) for TiN coated specimens

Nevertheless, the corrosion essence of the coatings is generally considered because aggressive electrolytes diffuse to the substrate through defects (e.g., micropores and pinholes) in the coatings and lead to corrosion [16, 40]. Additionally, TiN coatings inevitably contain defects [40]. Therefore, additional work on the corrosion evolution of TiN coatings is necessary for the application of TiN-coated 310S in an electric water heater environment.

4. CONCLUSIONS

Dense TiN coating with a thickness of about 7 μm was prepared on 310S surface via magnetron sputtering. The growth orientation of TiN coating is mainly in the $\langle 1\ 1\ 1 \rangle$ direction with a columnar structure. The TiN coating shows excellent spontaneous passivation property in hot tap water and 3.5% NaCl solution. In comparison with the bare substrate, the corrosion potential, polarization resistance and pitting potential of TiN-coated specimens are obviously higher. Clearly, the TiN coatings can significantly enhance the pitting corrosion resistance of 310S stainless steel in aggressive environments containing Cl^- such as hot tap water and brine solutions. These indicate that the TiN coating may be a suitable choice for the corrosion protection of heating tubes in electric water heater.

References

1. M.H. Nazari, Y. Zhang, A. Mahmoodi, G. Xu, J. Y, J.L. Wu, X.M. Shi, *Prog. Org. Coat.*, 162 (2022) 106573.
2. X.H. Chen, C.S. Chen, H.N. Xiao, F.Q. Cheng, G. Zhang, G.J. Yi, *Surf. Coat. Technol.*, 191 (2005) 351.
3. D.M. Zhang, L.T. Duan, L.Guo, W.H. Tuan, *Int. J. Hydrog. Energy*, 35 (2010) 3721.
4. S.A. Naghibi, K. Raeissi, M.H. Fathi, *Mater. Chem. Phys.*, 148 (2014) 614.
5. R. Ananthakumar, B. Subramaniana, A. Kobayashi, M. Jayachandran, *Ceram. Int.*, 38 (2012) 477.
6. G. Lazorenko, A. Kasprzhitskii, T. Nazdrachev, *Constr. Build. Mater.*, 288 (2021) 123115.
7. Y. Liu, J.J. Yang, H. Yang, K. Li, Y.T. Qiu, W.C. Zhang, S.F. Zhou, *Surf. Coat. Technol.*, 428 (2021) 127868.
8. M.H. Zeng, Y. Yang, M.C. Li, *Int. J. Electrochem. Sci.*, 16 (2021) 1.
9. R.Y., Zhang, X. Yu, Q.W. Yang, G. Cui, Z.L. Li, *Constr. Build. Mater.*, 294 (2021) 123613.
10. R.K. Gupta, N. Birbilis, *Corros. Sci.*, 92 (2015) 1.
11. H.E. Rebenne, D.G. Bhat, *Surf. Coat. Tech.*, 63 (1994) 1.
12. J.S. Meng, X.P. Shi, S.J. Zhang, M.Y. Wang, F. Xue, B.B. Liu, W.C. Cui, L.H. Bian, *Surf. Coat. Tech.*, 374 (2019) 437.
13. F. M. Alanagh, M. Mahdavi, *Surf. Interfaces*, 18 (2020) 100428.
14. T.D. Atmani, M. Gaceb, H. Aknouche, C. Nouveau, M.S. Bouamrene, *Surf. Interfaces*, 23 (2021) 101001.
15. S.T. Myung, M. Kumagai, R. Asaishi, Y.K. Sun, H. Yashiro, *Electrochem Commun*, 10 (2008) 480.
16. Y. Wang, D.O. Northwood, *Int. J. Hydrog. Energy*, 32 (2007) 895.
17. L. Wang, D.O. Northwood, X. Nie, J. Housden, E. Spain, A. Leyland, A. Matthews, *J. Power Sources*, 195 (2010) 3814.
18. R.M. Souto, H. Alanyali, *Corros. Sci.*, 42 (2000) 2201.
19. R. Li, S.H. Wang, D.P. Zhou, J.B. Pu, M. Yu, W.M. Guo, *Corros. Sci.*, 174 (2020) 108794.
20. M. Song, J.J. Guo, Y.F. Yang, K. Geng, M.Q. Xiang, Q.S. Zhu, C.Q. Hu, H.D. Zhao, *Appl. Surf. Sci.*, 504 (2020) 144483.
21. C.L. Liu, P.K. Chu, G.Q. Lin, D.Z. Yang, *Corros. Sci.*, 49 (2007) 3783.
22. F.C. Silva, O.M. P. Ramirez, M.A. Tunes, P.D. Edmondson, J.C. Sagás, L.C. Fontana, H.G. Melo, C.G. Schön, *Int. J. Hydrog. Energy*, 45 (2020) 33993.
23. N. F. Asri, T. Husaini, A.B. Sulong, E.H. Majlan, W.R.W. Daud, *Int. J. Hydrog. Energy*, 42 (2017) 9135.
24. R.J. Tian, J.C. Sun, *Int. J. Hydrog. Energy*, 36 (2011) 6788.
25. N.D. Nam, D.S. Jo, J.G. Kim, D.H. Yoon, *Thin Solid Films*, 519 (2011) 6787.

26. P.P. Gao, Z.Y. Xie, X.B. Wu, C. Ouyang, T. Lei, P.P. Yang, C.B. Liu, J.B. Wang, T. Ouyang, Q.Z. Huang, *Int. J. Hydrog. Energy*, 43 (2018) 20947.
27. M.J. Zhang, R.H. Xu, L.L. Liu, S.S. Xin, M.C. Li, *Anti-Corros Method M*, 67 (2020) 407.
28. L. A. Dobrzański, K. Lukaszewicz, A. Zarychta, L. Cunha, *J. Mater. Process. Technol.*, 164 (2005) 816.
29. C.H. Hsu, M.L. Chen, K.L. Lai, *Mater. Sci. Eng. A*, 421 (2006) 182.
30. C.L. Liu, D.Z. Yang, G.Q. Lin, M. Qi, *Mater. Lett.*, 59 (2005) 3813.
31. Y. Wang, D.O. Northwood, *J. Power Sources*, 165 (2007) 293.
32. C.M. Abreu, M.J. Cristóbal, R. Losada, X.R. Nóvoa, G. Pena, M.C. Pérez, *Electrochim. Acta*, 51 (2006) 1881.
34. R.J. Jiang, Y.W. Wang, X. Wen, C.F. Chen, J.M. Zhao, *Appl. Surf. Sci.*, 412 (2017) 214.
35. Y. Yang, H.T. Zeng, S.S. Xin, X.L. Hou, M.C. Li, *Corros. Sci.*, 165 (2020) 108383.
36. M.C. Li, S.Z. Luo, P.F. Wu, J.N. Shen, *Electrochim. Acta*, 50 (2005) 3401.
37. J. Ninlachart, K.S. Raja, *Acta Metall. Sin.-Engl. Lett.*, 30 (2017) 352.
38. X.Q. Cheng, Y. Wang, X.G. Li, C.F. Dong, *J. Mater. Sci. Technol.*, 34 (2018) 2140.
39. J. Liao, K. Kishimoto, M. Yao, Y. Mori, M. Ikai, *Corros. Sci.*, 55 (2012) 205.
40. P. Ernst, N. J. Laycock, M. H. Moayed, R. C. Newman, *Corros. Sci.*, 39 (1997) 1133.
41. M.C. Li, S.Z. Luo, C.L. Zeng, J.N. Shen, H.C. Lin, C.N. Cao, *Corros. Sci.*, 46 (2004) 1369.

© 2022 The Authors. Published by ESG (www.electrochemsci.org). This article is an open access article distributed under the terms and conditions of the Creative Commons Attribution license (<http://creativecommons.org/licenses/by/4.0/>).